Editors' Suggestion

Topology of Disconnected Elementary Band Representations

Jennifer Cano,[1] Barry Bradlyn,[1] Zhijun Wang,[2] L. Elcoro,[3] M. G. Vergniory,[4,5]
C. Felser,[6] M. I. Aroyo,[3] and B. Andrei Bernevig[2,4,7,*]
[1]Princeton Center for Theoretical Science, Princeton University, Princeton, New Jersey 08544, USA
[2]Department of Physics, Princeton University, Princeton, New Jersey 08544, USA
[3]Department of Condensed Matter Physics, University of the Basque Country UPV/EHU, Apartado 644, 48080 Bilbao, Spain
[4]Donostia International Physics Center, P. Manuel de Lardizabal 4, 20018 Donostia-San Sebastián, Spain
[5]Department of Applied Physics II, University of the Basque Country UPV/EHU, Apartado 644, 48080 Bilbao, Spain
and Ikerbasque, Basque Foundation for Science, 48013 Bilbao, Spain
[6]Max Planck Institute for Chemical Physics of Solids, 01187 Dresden, Germany
[7]Laboratoire Pierre Aigrain, Ecole Normale Supérieure-PSL Research University,
CNRS, Université Pierre et Marie Curie-Sorbonne Universités, Université Paris Diderot-Sorbonne Paris Cité,
24 rue Lhomond, 75231 Paris Cedex 05, France,
Sorbonne Universités, UPMC Univ Paris 06, UMR 7589, LPTHE, F-75005, Paris, France,
and LPTMS, CNRS (UMR 8626), Université Paris-Saclay, 15 rue Georges Clémenceau, 91405 Orsay, France

(Received 17 January 2018; published 27 June 2018)

Elementary band representations are the fundamental building blocks of atomic limit band structures. They have the defining property that at partial filling they cannot be both gapped and trivial. Here, we give two examples—one each in a symmorphic and a nonsymmorphic space group—of elementary band representations realized with an energy gap. In doing so, we explicitly construct a counterexample to a claim by Michel and Zak that single-valued elementary band representations in nonsymmorphic space groups with time-reversal symmetry are connected. For each example, we construct a topological invariant to explicitly demonstrate that the valence bands are nontrivial. We discover a new topological invariant: a movable but unremovable Dirac cone in the "Wilson Hamiltonian" and a bent-$\mathbb{Z}_2$ index.

DOI: 10.1103/PhysRevLett.120.266401

The theory of topological quantum chemistry introduced in Ref. [1] diagnoses topological phases based on elementary band representations. A set of bands is topological if it lacks an "atomic limit" that obeys the crystal symmetry (and time reversal, if desired): formally, an atomic limit exhibits a set of localized, symmetric Wannier functions [1–7]. This definition includes all known topological insulating phases [8–18]. We showed in Refs. [1,2] that each atomic limit defines a "band representation," which is a representation of the full space group. The irreducible representations (irreps) of the little group at each point in the Brillouin zone are completely determined for each band representation [19–21]. However, the little group irreps do not define the band representation: two groups of bands can exhibit the same little group irreps but differ by a Berry phase [2,22–24].

If a set of bands, separated by an energy gap from all other bands, does not transform as a band representation, it does not have localized, symmetric Wannier functions; consequently, it is topological [1,2]. An "elementary" band representation (EBR) is not equivalent to a sum of two band representations. It follows that a disconnected (gapped) elementary band representation must realize a set of topological bands [1–3]. Such disconnected EBRs will be the focus of this Letter. All EBRs and their irreps at high-symmetry points in the Brillouin zone can be found on the Bilbao Crystallographic Server [1,25–30].

The theory of topological quantum chemistry also brings to light the different types of trivial-to-topological phase transitions, distinguished by how many symmetry-distinct orbitals contribute to the topological bands. For example, the Kane-Mele model of graphene [8] requires only one type of symmetry-distinct orbital (the two spinful p_z orbitals per unit cell are related by the honeycomb lattice symmetry), while the trivial-to-topological transition in HgTe [13] requires both s and p orbitals to create a "band inversion." These two types of topological insulators differ in their atomic limit as the distance between atoms is taken to infinity: in the atomic limit of graphene, the band structure consists of a single flat and fourfold degenerate band, corresponding to a single EBR. In contrast, in HgTe, the atomic limit will consist of two flatbands, one each for the s and p orbitals, corresponding to two distinct EBRs.

In this Letter, we will focus on the graphenelike case: topological insulators that derive from a single orbital and its symmetry-related partners. In the language of band representations, the conduction and valence bands together transform as a single EBR; consequently, either the conduction or valence bands (or both) lack an atomic limit and are topological [1–3].

We introduce models in a symmorphic and a nonsymmorphic space group. The symmorphic example describes $p_{x,y}$ orbitals on the honeycomb lattice. Without spin-orbit coupling (SOC), the band structure can be a (gapped) topological crystalline insulator (TCI). With infinitesimal SOC and time-reversal symmetry, the system exhibits a nontrivial $\mathbb{Z}_2$ index.

We were motivated to explore the nonsymmorphic example because, as part of their ground-breaking work on the connectivity of energy bands, Michel and Zak conjectured that spinless EBRs in nonsymmorphic space groups cannot realize a gapped band structure [31,32]. In Ref. [26], we explained where the proof of Michel and Zak fails. Here, we pick a particular nonsymmorphic space group, $P4_232$, and construct a tight-binding model to explicitly show its gapped, topological nature. In doing so, we find a novel feature: the two-dimensional "Wilson Hamiltonian" exhibits a topologically protected band crossing.

In each example, we derive a bulk topological invariant. An essential tool is the "$k_\parallel$-directed" Wilson loop, which describes the parallel transport of an isolated set of bands [4,17,33–42]:

$$\mathcal{W}_{(k_\perp,k_0)} \equiv P e^{i\int_{k_0}^{k_0+2\pi} dk_\parallel A_\parallel(k_\perp,k_\parallel)}, \tag{1}$$

where P indicates that the integral is path ordered and $A_\parallel(\mathbf{k})_{ij} = i\langle u_i(\mathbf{k})|\partial_{k_\parallel} u_j(\mathbf{k})\rangle$ is a matrix whose rows and columns correspond to each eigenstate in the isolated set of bands. The eigenvalues of $\mathcal{W}$ are gauge invariant and of the form $e^{i\theta(k_\perp)}$, independent of the "base point" k_0 [40]. A quantized invariant derived from the Wilson loop is invariant under any deformation of the Hamiltonian that preserves the gap in the spectrum.

Spinless TCI on the honeycomb lattice.—We start with spinless $p_{x,y}$ orbitals on the honeycomb lattice, described by the nearest-neighbor Hamiltonian [43]:

$$H^0_{\mathbf{k}} = \begin{pmatrix} 0 & h_{\mathbf{k}} \\ h^\dagger_{\mathbf{k}} & 0 \end{pmatrix}, \tag{2}$$

where nonzero blocks mix the A and B sublattices and

$$\begin{aligned} h_{\mathbf{k}} = {} & \frac{1}{2}(e^{-i\mathbf{k}\cdot\delta_1} + e^{-i\mathbf{k}\cdot\delta_2} + e^{-i\mathbf{k}\cdot\delta_3})(t_\sigma + t_\pi)\mathbb{I} \\ & + \frac{1}{2}\left(e^{-i\mathbf{k}\cdot\delta_1} - \frac{1}{2}e^{-i\mathbf{k}\cdot\delta_2} - \frac{1}{2}e^{-i\mathbf{k}\cdot\delta_3}\right)(t_\sigma - t_\pi)\sigma_z \\ & + \frac{\sqrt{3}}{4}(e^{-i\mathbf{k}\cdot\delta_2} - e^{-i\mathbf{k}\cdot\delta_3})(t_\sigma - t_\pi)\sigma_x. \end{aligned} \tag{3}$$

The Pauli matrices $\sigma_{x,y,z}$ act in the $p_{x,y}$ subspace, $t_{\sigma,\pi}$ parametrize σ and π bond strengths, and $\delta_{1,2,3}$ are the nearest-neighbor vectors [see Fig. 1(a)]. Previously this model with $t_\pi = 0$ was studied for its flatbands [44,45].

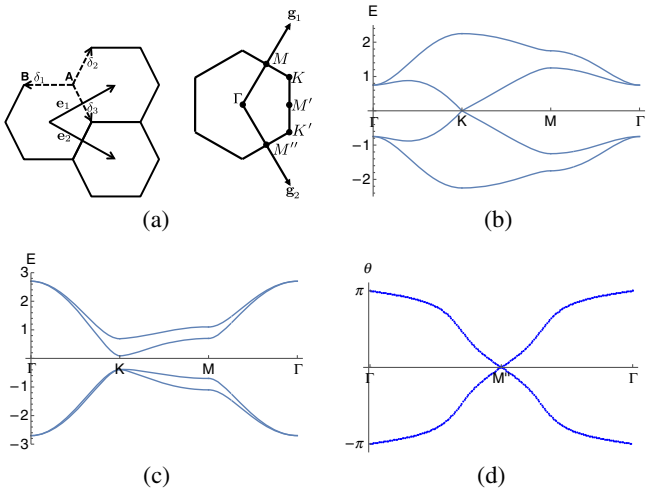

FIG. 1. (a) Lattice ($\mathbf{e}_{1,2}$) and reciprocal lattice ($\mathbf{g}_{1,2}$) basis vectors. The dotted arrows ($\delta_{1,2,3}$) indicate the vectors between nearest neighbor sites. **A** and **B** indicate the sublattices. (b) Spectrum of $H^0_{\mathbf{k}}$ with $t_\sigma = 1$, $t_\pi = -0.5$. (c) Gapped band structure of $H^0_{\mathbf{k}} + xH^1_{\mathbf{k}}$ with $t_\sigma = 0.8$, $t_\pi = 1.0$, $x = 0.6$, and (d) the argument of its Wilson loop eigenvalues.

The spectrum of $H^0_{\mathbf{k}}$ is shown in Fig. 1(b). The degeneracies at $K \equiv \frac{2}{3}\mathbf{g}_1 + \frac{1}{3}\mathbf{g}_2$ and Γ are symmetry required [46].

To open a gap, we add the following next-nearest neighbor hopping term, which preserves the crystal symmetries of the honeycomb lattice [47]:

$$H^1_{\mathbf{k}} = \sin\left(\frac{1}{2}\mathbf{k}\cdot\mathbf{e}_1\right)\sin\left(\frac{1}{2}\mathbf{k}\cdot\mathbf{e}_2\right)\sin\left[\frac{1}{2}\mathbf{k}\cdot(\mathbf{e}_1 - \mathbf{e}_2)\right]\tau_z \otimes \sigma_y, \tag{4}$$

where the matrices τ_i act in the sublattice subspace. The term in Eq. (4) changes the energy ordering of the bands at K, while preserving the twofold degeneracy. For large enough $|x|$, $H^0_{\mathbf{k}} + xH^1_{\mathbf{k}}$ can be gapped, as in Fig. 1(c); see Sec. S1 A in Supplemental Material [47] for a phase diagram.

The spectrum in Fig. 1(c) represents a disconnected EBR [1,2]. We construct a nontrivial bulk topological invariant from the $\mathbf{g}_1$-directed Wilson loop of the lower two bands. Its eigenvalues are shown in Fig. 1(d) as a function of the base point. When the base point is Γ or M, the Wilson loop eigenvalues (-1 and $+1$, respectively [47]) are completely determined by the C_{2z} eigenvalues [38,42] (the C_{2z} operator is $-\tau_x \otimes \sigma_0$ [48]). This forces the "Wilson bands" to wind in opposite directions. The quantized eigenvalues at Γ and M prevent the Wilson spectrum from being smoothly deformed to flat, which indicates that the valence bands are topologically nontrivial.

The Wilson loop winding requires that both occupied bands of $H^0_{\mathbf{k}} + xH^1_{\mathbf{k}}$ at Γ have the same C_{2z} eigenvalue, η, and that both occupied bands at M have the C_{2z} eigenvalue, $-\eta$. Consider the Wilson loop of three bands: the two

occupied bands and a third, trivial, band, not in our model. If the C_{2z} eigenvalues of the third band at Γ and M are both equal to η, then the eigenvalues of the three-band Wilson loop will not be quantized at M and it will fail to wind. Thus, the topological invariant is not stable to adding a third band to the projector (although the winding of the projector onto two bands *is* invariant under adding a third band as long as the gap between the third band and the existing bands does not close). The existence of a topological invariant that depends on the number of bands is reminiscent of the "Hopf insulator" [49].

Spinful topological phases.—We now consider SOC. Spinful $p_{x,y}$ orbitals decompose into three irreps of the site-symmetry group. Bands derived from these three irreps transform as a sum of three EBRs [1,2], which generically split into four sets of disconnected bands, as in Figs. 2(a) and 2(b). At least one set of disconnected bands is either an obstructed atomic limit—it can be adiabatically deformed to a Hamiltonian composed of orbitals that reside at the center of the hexagon rather than the corners—or a topological band that does not have any atomic limit [50].

If time-reversal symmetry is enforced, we can consider the $\mathbb{Z}_2$ index. For small spin-conserving SOC that does not invert the bands at Γ or M, the C_{2z} eigenvalues in the spinless phase determine the $\mathbb{Z}_2$ index of each set of bands (conserving spin amounts to enforcing inversion symmetry). Our simple, but physically motivated, model yields two phases, shown in Fig. 2: either all three or the first and third gaps are $\mathbb{Z}_2$ topological, while the middle gap is not;

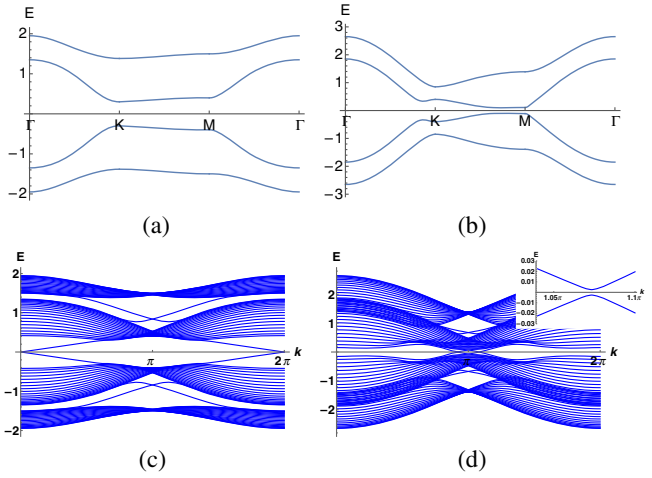

FIG. 2. Band structures with an on-site $L \cdot S$ term for (a),(b) periodic and (c),(d) slab boundary conditions. This SOC term preserves inversion symmetry, such that all bands remain doubly degenerate, but is general enough to open all possible gaps in the band structure. In (a) only the lowest and highest bands have a nontrivial $\mathbb{Z}_2$ index and hence the slab boundary conditions in (c) reveal edge states in all three gaps. In (b) all four bands have a nontrivial $\mathbb{Z}_2$ index and hence the slab boundary conditions in (d) reveal edge states in only the upper and lower gaps. The inset in (d) resolves the avoided crossing at $E = 0$.

there is no phase in which all gaps are $\mathbb{Z}_2$ trivial [51]. We show in Sec. S1 C of Ref. [51] that only spin-conserving SOC can open a gap in the spinless band structure; hence, if non-spin-conserving SOC is present and does not invert any bands, it will alter the band structure but not change the $\mathbb{Z}_2$ index.

Material realization.—The spinless semimetallic model $H^0_{\mathbf{k}}$ consists of nearest-neighbor Slater-Koster [52] terms; thus, it is widely applicable to two-dimensional planar honeycomb systems. To exhibit the TCI phase, the next-nearest neighbor term $H^1_{\mathbf{k}}$ must be dominant in order to open a gap. The relative strength of the hopping terms varies with strain or buckling.

The nontrivial $\mathbb{Z}_2$ phases will be present whenever SOC is large enough to open an observable gap, but not so large to invert the bands at Γ and M. In particular, $H^0_{\mathbf{k}}$ with SOC describes bismuth grown on a SiC substrate, consistent with the topological edge states reported in Ref. [53].

Nonsymmorphic gapped EBR.—We now consider the nonsymmorphic simple cubic space group $P4_232$, which is generated by $\{C_{2x}|\mathbf{0}\}$, $\{C_{3,111}|\mathbf{0}\}$, and $\{C_{2,110}|\frac{1}{2}\frac{1}{2}\frac{1}{2}\}$. We also enforce time-reversal symmetry. We consider atoms sitting at (0,0,0) and $(\frac{1}{2},\frac{1}{2},\frac{1}{2})$ [inset of Fig. 3(a)], which together comprise the $2a$ Wyckoff position, each with spinless d_{z^2} and $d_{x^2-y^2}$ orbitals, which together form a time-reversal symmetric irrep of the site-symmetry group [54,55]. Since the orbitals transform as an irrep of a maximal Wyckoff position, any band structure derived from these orbitals transforms as a time-reversal invariant EBR. It follows from Ref. [2] that if the band structure is gapped, it contains topological bands. Here, we explicitly construct a gapped Hamiltonian and a nontrivial bulk topological invariant, violating the conjecture [31,32] that a single set of symmetry-related orbitals in a nonsymmorphic space group always yields a gapless band structure.

We consider the following Hamiltonian, which respects all space group symmetries and time reversal [56]:

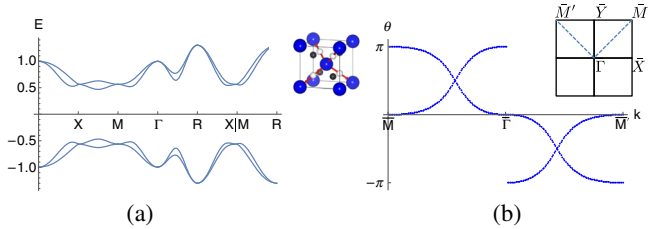

FIG. 3. (a) Spectrum of $H_{\mathbf{k}} + H^1_{\mathbf{k}}$ with $t_1 = 0.2$, $t_2 = 0.3$, $t_3 = 0.1$, $t_4 = 0.08$, $t_5 = 0.05$, $t_6 = 0.02$. Inset shows unit cell: orbitals on the blue atoms enter the Hamiltonian, while the white or black atoms create a crystal field with the symmetry of $P4_232$. (b) Argument of the eigenvalues of the z-directed Wilson matrix along the path $\bar{M} - \bar{\Gamma} - \bar{M}'$ (blue dotted line in inset); $\bar{M} = (\pi, \pi)$, $\bar{\Gamma} = (0, 0)$, $\bar{M}' = (-\pi, \pi)$.

$$H_{\mathbf{k}} = t_1 f_1(\mathbf{k})\tau_x \otimes \sigma_0 + t_2 f_2(\mathbf{k})\tau_y \otimes \sigma_0 + t_3(g_1(\mathbf{k})\tau_z \otimes \sigma_z + g_2(\mathbf{k})\tau_z \otimes \sigma_x), \quad (5)$$

where $f_1(\mathbf{k}) = \sum_i \cos(\mathbf{k}\cdot\delta_i)$, $f_2(\mathbf{k}) = \sum_i \sin(\mathbf{k}\cdot\delta_i)$, $g_1(\mathbf{k}) = \cos k_x - \cos k_y$, $g_2(\mathbf{k}) = (\cos k_x + \cos k_y - 2\cos k_z)/\sqrt{3}$, and $\delta_{1,2,3,4}$ are vectors to nearest neighbors, shown in Fig. 3(a). The band structure is doubly degenerate and gapped when $t_{1,2,3} \neq 0$. To eliminate the extra degeneracies, we add the symmetry-preserving term

$$H^1_{\mathbf{k}} = t_4 f_1(\mathbf{k})\tau_y \otimes \sigma_y + t_5\tau_0 \otimes [g_2(\mathbf{k})\sigma_z - g_1(\mathbf{k})\sigma_x] + t_6 g_3(\mathbf{k})\tau_z \otimes \sigma_0, \quad (6)$$

where

$$g_3(\mathbf{k}) = \cos(2k_x)\cos(k_y) - \cos(2k_y)\cos(k_x) + \text{perm}, \quad (7)$$

and "+perm" indicates terms obtained by permuting $k_x \to k_y \to k_z$. The spectrum of $H_{\mathbf{k}} + H^1_{\mathbf{k}}$ is shown in Fig. 3(a). Since $H_{\mathbf{k}}$ is fully gapped when $t_{1,2,3} \neq 0$, $H_{\mathbf{k}} + H^1_{\mathbf{k}}$ is gapped when $t_{4,5,6}$ are small compared to $t_{1,2,3}$.

This gapped phase realizes a disconnected and time-reversal symmetric EBR; thus, it contains topological bands. We diagnose the topological phase by the winding of its z-directed Wilson loop along the *bent* path shown in Fig. 3(b). This is a time-reversal symmetric and nonsymmorphic generalization of the "bent Chern number" introduced in Ref. [57]. Two features are necessary for this loop to wind: first, the Wilson loop eigenvalues are pinned to ± 1 at $\bar{\Gamma}$ and $\bar{M}$, and, second, there are protected band crossings in the Wilson spectrum along the $|k_x| = |k_y|$ lines. Combined, these features prevent the Wilson bands from being smoothly deformable to flatbands; hence, the phase is topological.

We now explain the origin of these features: first, C_{2x} symmetry forces the eigenvalues of $\mathcal{W}_{(\bar{\Gamma},0)}$ and $\mathcal{W}_{(\bar{M},0)}$ to be real, while the $\{C_{2,110}|\frac{1}{2}\frac{1}{2}\frac{1}{2}\}$ screw symmetry forces them to come in pairs $(\lambda, -\lambda^*)$ [58]. This combination pins the eigenvalues of $\mathcal{W}_{(k_x,k_y,0)}$ to be ± 1 at $\bar{\Gamma}$ and $\bar{M}$.

The Wilson band crossing is subtle: the $\{C_{2,110}|\frac{1}{2}\frac{1}{2}\frac{1}{2}\}$ screw symmetry requires the eigenvalues of $\mathcal{W}_{(k,k,0)}$ to come in pairs $(\lambda, -\lambda^*)$. Combined with the antiunitary symmetry $\mathcal{T}\{C_{2,110}|\frac{1}{2}\frac{1}{2}\frac{1}{2}\}^{-1}C_{2z}$, which leaves points (k,k,k_z) invariant, the Wilson matrix must take the form $\mathcal{W}_{(k,k,0)} = ie^{ia_x(k)\sigma_x + ia_y(k)\sigma_y}$, where, importantly, $a_x(k) \propto a_y(k)$ [alternately, the symmetries permit the eigenvalues of $\mathcal{W}_{(k,k,0)}$ to be fixed to ± 1; see Sec. S3 B]. Then degeneracies of the Wilson eigenvalues, which occur when $a_x(k) = a_y(k) = 0$, are not fine-tuned, since the symmetry forced $a_x(k) \propto a_y(k)$. Since the eigenvalues of $\mathcal{W}_{(k,k,0)}$ at $k = 0$ and $k = \pi$ are fixed to $+1$ and -1, an odd number of linear degeneracies between $\bar{\Gamma}$ and $\bar{M}$ cannot be removed without closing the bulk band gap. Thus, the parity of the number of linear degeneracies is a topological invariant.

The band crossing forms a Dirac cone in the two-dimensional Wilson Hamiltonian [40]. The Dirac point is revealed by the Berry phase w acquired by an eigenstate of $\mathcal{W}_{(k_x,k_y,0)}$ as it traverses the path γ around the Dirac point. The Berry phase of Wilson loop eigenstates was introduced in Ref. [41]. Since w is quantized to ± 1 (see Sec. S4), it constitutes a topological invariant. In our model, for several values of parameters, we have numerically computed the nontrivial value, $w = -1$.

When SOC is present, the spinful d_{z^2} and $d_{x^2-y^2}$ orbitals transform as spin-$\frac{3}{2}$ orbitals, which induce an eight-band time-reversal symmetric EBR [27]. When the EBR is gapped, the valence (or conduction) bands must be topological.

Weak symmetry indicators.—In both the spinless TCI on the honeycomb lattice and the nonsymmorphic gapped EBR, the valence bands are topological, but have the property that the irreps at high-symmetry points can be written as a "difference" of the irreps in two other EBRs [59]. Because the irreps can be written as a difference, classification schemes [60] that treat the little group irreps as a vector space will identify the valence bands as trivial, even though they lack an atomic limit. However, unless an energy gap closes to the valence bands, the winding of the Wilson loop in both examples provides a robust and quantized topological invariant that is, in principle, physically observable [42,61,62].

This distinction warrants a refined characterization of topological crystalline bands based on whether their topological nature can be deduced by their little group irreps. We label the symmetry properties of topological bands as strong if their little group irreps are not equal to a linear combination of little group irreps corresponding to EBRs and weak if their little group irreps are equal to a difference (but not a sum) of irreps in EBRs. Strong symmetry properties implies a stable topological index; however, the converse is not true: for example, bands with a nontrivial $\mathbb{Z}_2$ index under time-reversal symmetry can be strong [10] or weak [1]. This usage of weak and strong symmetry is different than the current distinction between weak and strong topological insulators [10]. It is more suitable for the refined classification of topological insulators with crystal symmetries.

Conclusions.—We have constructed tight-binding models to realize the insulating phases of two gapped EBRs. We explicitly showed that the valence bands have a nontrivial topological invariant. In doing so, we found a new topological invariant in a nonsymmorphic space group: a Dirac cone in the Wilson loop spectrum and a Wilson loop that winds along a bent path. This motivates further study of the gapped EBRs in other nonsymmorphic space groups. In addition, we introduced the notion of a weak symmetry indicator. We postpone a general investigation of the symmetry properties of gapped EBRs to future work.

B. B., J. C., Z. W., and B. A. B. acknowledge the hospitality of the Donostia International Physics Center. B. A. B. acknowledges the hospitality and support of the École Normale Supérieure and Laboratoire de Physique Théorique et Hautes Energies. The work of M. G. V. was supported by FIS2016-75862-P. The work of L. E. and M. I. A. was supported by the Government of the Basque Country (Project No. IT779-13) and the Spanish Ministry of Economy and Competitiveness and FEDER funds (Project No. MAT2015-66441-P). B. A. B. acknowledges the support of the NSF EAGER Award Nos. DMR-1643312, ONR-N00014-14-1-0330, NSF-MRSEC DMR-1420541, ARO MURI W911NF-12-1-0461, the Department of Energy de-sc0016239, the Simons Investigator Award, Packard Foundation, and the Schmidt Fund for Innovative Research.

*Permanent address: Department of Physics, Princeton University, Princeton, New Jersey 08544, USA.

[1] B. Bradlyn, L. Elcoro, J. Cano, M. G. Vergniory, Z. Wang, C. Felser, M. I. Aroyo, and B. A. Bernevig, Nature (London) **547**, 298 (2017).
[2] J. Cano, B. Bradlyn, Z. Wang, L. Elcoro, M. G. Vergniory, C. Felser, M. I. Aroyo, and B. A. Bernevig, Phys. Rev. B **97**, 035139 (2018).
[3] H. C. Po, H. Watanabe, and A. Vishwanath, arXiv:1709.06551.
[4] A. A. Soluyanov and D. Vanderbilt, Phys. Rev. B **83**, 035108 (2011).
[5] A. A. Soluyanov and D. Vanderbilt, Phys. Rev. B **85**, 115415 (2012).
[6] N. Marzari, A. A. Mostofi, J. R. Yates, I. Souza, and D. Vanderbilt, Rev. Mod. Phys. **84**, 1419 (2012).
[7] N. Read, Phys. Rev. B **95**, 115309 (2017).
[8] C. L. Kane and E. J. Mele, Phys. Rev. Lett. **95**, 226801 (2005).
[9] J. E. Moore and L. Balents, Phys. Rev. B **75**, 121306 (2007).
[10] L. Fu and C. L. Kane, Phys. Rev. B **76**, 045302 (2007).
[11] L. Fu, C. L. Kane, and E. J. Mele, Phys. Rev. Lett. **98**, 106803 (2007).
[12] R. Roy, Phys. Rev. B **79**, 195322 (2009).
[13] B. A. Bernevig, T. L. Hughes, and S.-C. Zhang, Science **314**, 1757 (2006).
[14] J. C. Y. Teo, L. Fu, and C. L. Kane, Phys. Rev. B **78**, 045426 (2008).
[15] L. Fu, Phys. Rev. Lett. **106**, 106802 (2011).
[16] K. Shiozaki, M. Sato, and K. Gomi, Phys. Rev. B **95**, 235425 (2017).
[17] B. J. Wieder, B. Bradlyn, Z. Wang, J. Cano, Y. Kim, H.-S. D. Kim, A. M. Rappe, C. L. Kane, and B. A. Bernevig, arXiv:1705.01617.
[18] H. Song, S.-J. Huang, L. Fu, and M. Hermele, Phys. Rev. X **7**, 011020 (2017).
[19] J. Zak, Phys. Rev. Lett. **45**, 1025 (1980).
[20] J. Zak, Phys. Rev. B **26**, 3010 (1982).
[21] H. Bacry, L. Michel, and J. Zak, Symmetry and classification of energy bands in crystals, in *Group Theoretical Methods in Physics: Proceedings of the XVI International Colloquium, Varna, Bulgaria, 1987* (Springer, Berlin, 1988), p. 289.
[22] H. Bacry, L. Michel, and J. Zak, Phys. Rev. Lett. **61**, 1005 (1988).
[23] H. Bacry, Commun. Math. Phys. **153**, 359 (1993).
[24] L. Michel and J. Zak, Europhys. Lett. **18**, 239 (1992).
[25] B. Bradlyn, L. Elcoro, M. G. Vergniory, J. Cano, Z. Wang, C. Felser, M. I. Aroyo, and B. A. Bernevig, Phys. Rev. B **97**, 035138 (2018).
[26] M. G. Vergniory, L. Elcoro, Z. Wang, J. Cano, C. Felser, M. I. Aroyo, B. A. Bernevig, and B. Bradlyn, Phys. Rev. E **96**, 023310 (2017).
[27] L. Elcoro, B. Bradlyn, Z. Wang, M. G. Vergniory, J. Cano, C. Felser, B. A. Bernevig, D. Orobengoa, G. de la Flor, and M. I. Aroyo, J. Appl. Crystallogr. **50**, 1457 (2017).
[28] M. I. Aroyo, J. M. Perez-Mato, D. Orobengoa, E. Tasci, G. de la Flor, and A. Kirov, Bulg. Chem. Commun. **43**, 183 (2011).
[29] M. I. Aroyo, J. M. Perez-Mato, C. Capillas, E. Kroumova, S. Ivantchev, G. Madariaga, A. Kirov, and H. Wondratschek, Z. Kristallogr. **221**, 15 (2006).
[30] M. I. Aroyo, A. Kirov, C. Capillas, J. M. Perez-Mato, and H. Wondratschek, Acta Crystallogr. Sect. A **62**, 115 (2006).
[31] L. Michel and J. Zak, Phys. Rev. B **59**, 5998 (1999).
[32] L. Michel and J. Zak, Phys. Rep. **341**, 377 (2001).
[33] J. Zak, Phys. Rev. Lett. **62**, 2747 (1989).
[34] L. Fu and C. L. Kane, Phys. Rev. B **74**, 195312 (2006).
[35] S. Ryu, C. Mudry, H. Obuse, and A. Furusaki, New J. Phys. **12**, 065005 (2010).
[36] R. Yu, X. L. Qi, A. Bernevig, Z. Fang, and X. Dai, Phys. Rev. B **84**, 075119 (2011).
[37] M. Taherinejad, K. F. Garrity, and D. Vanderbilt, Phys. Rev. B **89**, 115102 (2014).
[38] A. Alexandradinata, X. Dai, and B. A. Bernevig, Phys. Rev. B **89**, 155114 (2014).
[39] Z. Wang, A. Alexandradinata, R. J. Cava, and B. A. Bernevig, Nature (London) **532**, 189 (2016).
[40] A. Alexandradinata, Z. Wang, and B. A. Bernevig, Phys. Rev. X **6**, 021008 (2016).
[41] W. A. Benalcazar, B. A. Bernevig, and T. L. Hughes, Science **357**, 61 (2017).
[42] J. Höller and A. Alexandradinata, arXiv:1708.02943.
[43] See Supplemental Material at http://link.aps.org/supplemental/10.1103/PhysRevLett.120.266401, Sec. S1, for the derivation of Eqs. (2) and (3).
[44] C. Wu, D. Bergman, L. Balents, and S. Das Sarma, Phys. Rev. Lett. **99**, 070401 (2007).
[45] Z. Liu, Z.-F. Wang, J.-W. Mei, Y.-S. Wu, and F. Liu, Phys. Rev. Lett. **110**, 106804 (2013).
[46] E. Kogan and V. U. Nazarov, Phys. Rev. B **85**, 115418 (2012).
[47] See Supplemental Material at http://link.aps.org/supplemental/10.1103/PhysRevLett.120.266401, Sec. S1 A, for the possible C_{2z} eigenvalues.
[48] See Supplemental Material at http://link.aps.org/supplemental/10.1103/PhysRevLett.120.266401, Sec. S1, for the enumeration of the crystal symmetries of the honeycomb lattice.

[49] J. E. Moore, Y. Ran, and X.-G. Wen, Phys. Rev. Lett. **101**, 186805 (2008).
[50] See Supplemental Material at http://link.aps.org/supplemental/10.1103/PhysRevLett.120.266401, Sec. S1 C, for a description of the possibilities.
[51] See Supplemental Material at http://link.aps.org/supplemental/10.1103/PhysRevLett.120.266401, Sec. S1 C, for computation of the possible C_{2z} eigenvalues.
[52] J. C. Slater and G. F. Koster, Phys. Rev. **94**, 1498 (1954).
[53] F. Reis, G. Li, L. Dudy, M. Bauernfeind, S. Glass, W. Hanke, R. Thomale, J. Schäfer, and R. Claessen, Science **357**, 287 (2017).
[54] *International Tables for Crystallography*, Vol. A, edited by M. I. Aroyo (International Union of Crystallography, 2016).
[55] S. Altmann and P. Herzig, *Point-Group Theory Tables*, 2nd ed. (University of Vienna, Vienna, 2011).
[56] See Supplemental Material at http://link.aps.org/supplemental/10.1103/PhysRevLett.120.266401, Sec. S2, for the matrix form of the symmetries.
[57] A. Alexandradinata, C. Fang, M. J. Gilbert, and B. A. Bernevig, Phys. Rev. Lett. **113**, 116403 (2014).
[58] See Supplemental Material at http://link.aps.org/supplemental/10.1103/PhysRevLett.120.266401, Sec. S3 A, for symmetry constraints on the Wilson loop.
[59] See Supplemental Material at http://link.aps.org/supplemental/10.1103/PhysRevLett.120.266401, Sec. S1 B, for details of the honeycomb case.
[60] H. C. Po, A. Vishwanath, and H. Watanabe, Nat. Commun. **8**, 50 (2017).
[61] M. Atala, M. Aidelsburger, J. T. Barreiro, D. Abanin, T. Kitagawa, E. Demler, and I. Bloch, Nat. Phys. **9**, 795 (2013).
[62] S. Nakajima, T. Tomita, S. Taie, T. Ichinose, H. Ozawa, L. Wang, M. Troyer, and Y. Takahashi, Nat. Phys. **12**, 296 (2016).